PREPRINT 476

JANUARY 2018

Comparison of Different Splitting Techniques for the Isentropic Euler Equations

Klaus Kaiser[a,b], Jonas Zeifang[c], Jochen Schütz[b], Andrea Beck[c] and Claus-Dieter Munz[c]

Institut für Geometrie und Praktische Mathematik
Templergraben 55, 52062 Aachen, Germany

[a] IGPM, RWTH Aachen University, Templergraben 55, D-52062 Aachen
[b] Faculty of Sciences, Hasselt University, Agoralaan Gebouw D, BE-3590 Diepenbeek
[c] IAG, Universität Stuttgart, Pfaffenwaldring 21, D-70569 Stuttgart

Comparison of Different Splitting Techniques for the Isentropic Euler Equations

Klaus Kaiser[a,b], Jonas Zeifang[c], Jochen Schütz[b], Andrea Beck[c], Claus-Dieter Munz[c]

[a]*IGPM, RWTH Aachen University, Templergraben 55, D-52062 Aachen*
[b]*Faculty of Sciences, Hasselt University, Agoralaan Gebouw D, BE-3590 Diepenbeek*
[c]*IAG, Universität Stuttgart, Pfaffenwaldring 21,D-70569 Stuttgart*

Abstract

The isentropic Euler equations at low Mach number are inherently stiff equations. To deal with them numerically, one can hardly use explicit-in-time standard methods known from the 'compressible' world as the CFL condition dictates prohibitively small time steps. A technique that has become popular in recent years is the use of a convective flux splitting upon which stiff and non-stiff parts are identified that are then treated implicitly and explicitly, respectively. This leads to the well-known IMEX schemes. In this paper, we investigate multiple splittings to accurately and efficiently compute the low-Mach number case of the compressible isentropic Euler equations. Temporal discretization is done with IMEX Runge-Kutta methods, while for the spatial part, we rely on the discontinuous Galerkin spectral element method. For a general class of splittings, it is shown that the fully discrete method respects the low-Mach asymptotics. Subsequently, splittings are investigated and compared numerically for several test cases.

Keywords: discontinuous Galerkin spectral element, low Mach, IMEX Runge-Kutta, flux splitting, asymptotic consistency

1. Introduction

The non-dimensionalized Euler equations at a low Mach number ε constitute a singularly perturbed system of equations [20, 33, 26], and are given by

$$\begin{aligned} \rho_t + \nabla \cdot (\rho \boldsymbol{u}) &= 0, \\ (\rho \boldsymbol{u})_t + \nabla \cdot (\rho \boldsymbol{u} \otimes \boldsymbol{u}) + \frac{1}{\varepsilon^2} \nabla p &= 0, \end{aligned} \tag{1}$$

with the equation of state $p(\rho) := \kappa \rho^\gamma$ and $\kappa > 0$, $\gamma \geq 1$. ρ, $\boldsymbol{u}$ and p denote density, velocity and pressure. If one considers so-called well-prepared initial data, which amount to claiming that

$$\rho(t=0) = \text{const} + O(\varepsilon^2), \qquad \text{and} \quad \nabla \cdot (\rho \boldsymbol{u})(t=0) = O(\varepsilon), \tag{2}$$

one can show that there is a well-behaved limit as $\varepsilon \to 0$ [20]. However, for small but finite ε, wave speeds differ tremendously as the speed of sound tends to infinity. This has serious influences on the CFL condition and demands for explicit-in-time schemes an impractically small time step Δt. Many attempts have been made to overcome this issue, see the by far not exhaustive list [6, 7, 9, 10, 11, 14, 21, 22, 27, 32] and the references therein. In particular, the concept of using flux splittings, see, e.g., [7, 8, 12, 18, 21, 27, 30], to treat stiff parts implicitly and non-stiff parts explicitly, resulting in so-called IMEX schemes [1, 2, 4, 19], has been intensely studied. In previous work [17, 18, 29, 34], we developed a flux splitting based on the solution $(\rho_{(0)}, \boldsymbol{u}_{(0)})$ of the incompressible Euler equations. This solution can be seen as the formal limit of a solution to Equation (1) and is given by

$$\begin{aligned} \rho_{(0)} \equiv \text{const} > 0, \quad \nabla \cdot \boldsymbol{u}_{(0)} &= 0, \\ (\boldsymbol{u}_{(0)})_t + \nabla \cdot (\boldsymbol{u}_{(0)} \otimes \boldsymbol{u}_{(0)}) + \frac{\nabla p_{(2)}}{\rho_{(0)}} &= 0, \end{aligned} \tag{3}$$

with $p_{(2)}$ denoting the hydrodynamic pressure. The developed flux splitting, termed RS-IMEX (RS stands for reference solution), shows many favorable properties with respect to stability and accuracy of an overall method [17, 18, 29].

However, the computation of a solution to (3) is usually not a trivial endeavour. In this work we consider different variants of the RS-IMEX splitting and established splittings from literature [8, 12]. We generalize all the used splittings – the RS-IMEX as well as the ones due to Degond/Tang (DeTa) [8] and Haack/Jin/Liu (HJL) [12] – to cast them into a general framework. For this framework, we can show the very important asymptotic consistency property that guarantees the correctness of an algorithm also in the $\varepsilon \to 0$ limit. We compare those splittings in the framework of a discontinuous Galerkin spectral element discretization [13, 24] of Equation (1).

The paper is structured as follows: In Section 2, we introduce the employed discretization method. Furthermore, we review, generalize and extend splittings known from literature. In Section 3 it is shown that the fully discrete method is asymptotically consistent. Section 4 then shows numerical results for a variety of splittings including the comparison of performance. Section 5 offers conclusion and outlook.

2. IMEX discontinuous Galerkin method

In the following, we shortly review the discontinuous Galerkin spectral element method combined with an IMEX Runge-Kutta method. Furthermore, we detail the splittings used in this work. We assume that the differential equations are given on domain $\Omega \times [0, T]$, $\Omega \subset \mathbb{R}^{\dim}$ with dim the spatial dimension (in this work, $\dim \in \{2, 3\}$), and $T \in \mathbb{R}^+$ is the final time. Boundary conditions are chosen to be periodic.

2.1. Numerical method

In conservative form, the isentropic Euler equations Equation (1) can be written as

$$0 = \partial_t \boldsymbol{w} + \nabla \cdot \boldsymbol{f}(\boldsymbol{w}).$$

Given a suitable identification of 'stiff' and 'non-stiff' parts, the flux can be split into a part $\widetilde{\boldsymbol{f}}$ that is treated implicitly and a part $\widehat{\boldsymbol{f}}$ that is treated explicitly, i.e.,

$$0 = \partial_t \boldsymbol{w} + \nabla \cdot \boldsymbol{f}(\boldsymbol{w}) = \partial_t \boldsymbol{w} + \nabla \cdot \left(\widetilde{\boldsymbol{f}}(\boldsymbol{w}) + \widehat{\boldsymbol{f}}(\boldsymbol{w})\right).$$

While $\boldsymbol{f}$ does not explicitly depend on time and space, we allow $\widetilde{\boldsymbol{f}}$ and $\widehat{\boldsymbol{f}}$ to do so, but supress the explicit notation for the ease of presentation. Temporal discretization is performed using IMEX Runge-Kutta methods [1, 25], which are combinations of implicit and explicit Runge-Kutta schemes. Spatial discretization is done by applying the discontinuous Galerkin spectral element discretization [24] to the split equation as done in [34]. This discretization is based on the tensor-product of one-dimensional Lagrange polynomials and requires a proper choice of the numerical flux function for the treatment of discontinuities at the cell boundaries. A detailed description of the present spatial discretization method can be found in [13]. We assume that the temporal domain is separated into N intervals of size Δt, i.e.,

$$[0, T] = \bigcup_{n=1}^{N} [t^{n-1}, t^n] \qquad \text{with} \qquad 0 = t^0 < \ldots < t^n < \ldots < t^N = T,$$

and the spatial domain is separated into ne cells, i.e.,

$$\Omega = \bigcup_{k=1}^{ne} \overline{\Omega_k} \qquad \text{with} \qquad \Omega_k \cap \Omega_i = \emptyset \quad \forall k \neq i.$$

The set of all cells Ω_k is denoted by $\mathcal{T}$, the corresponding skeleton – the set of all cell boundaries – by $\partial\mathcal{T}$. Then, $\mathbb{P}_q(\Omega_k)$ denotes the polynomial space with polynomials of maximum degree $q \geq 0$ on every cell Ω_k. Based on this, the broken polynomial space on the complete spatial domain is defined in the standard way by

$$V_q := \{v \in L^2(\Omega) \ : \ v_{|\Omega_k} \in \mathbb{P}_q(\Omega_k) \ \forall \ k = 1, \ldots, ne\},$$

and for systems by

$$V_q^{\dim+1} := \bigtimes_{i=1}^{\dim+1} V_q.$$

Obviously, a function $\sigma \in V_q$ is not necessarily continuous over a cell boundary, therefore we define for a cell boundary value $x \in \partial\Omega_k$ the interior $(-)$ and exterior $(+)$ value by

$$\sigma^{\mp}(x) := \lim_{0<\delta\to 0} \sigma(x \mp \delta \boldsymbol{n}_k),$$

where $\boldsymbol{n}_k$ is the outward pointing normal vector for cell Ω_k. If we consider $\sigma \in V_q$ on an edge e independent of neighboring cells, then we assume that a general direction $\boldsymbol{n}_e$ is given and consequently

$$\sigma^{\mp}(x) := \lim_{0<\delta\to 0} \sigma(x \mp \delta \boldsymbol{n}_e).$$

Before we can define the final method, we introduce an additional notation for the ease of presentation. For the integrals over a whole domain, i.e., over all elements of $\mathcal{T}$, we define the somewhat non-standard notation

$$(\boldsymbol{a}, \boldsymbol{b})_{\mathcal{T}} := \sum_{k=1}^{ne} \int_{\Omega_k} \boldsymbol{a} \cdot \boldsymbol{b} \, \mathrm{d}x$$

and for integrals over all cell boundaries, i.e., over all elements of $\partial\mathcal{T}$, we define

$$\{\boldsymbol{a}, b\}_{\partial\mathcal{T}} := \sum_{k=1}^{ne} \int_{\partial\Omega_k} (\boldsymbol{a}^+ + \boldsymbol{a}^-)\, b \cdot \boldsymbol{n}_k \, \mathrm{d}s \qquad \text{and} \qquad [\![\boldsymbol{a}, b]\!]_{\partial\mathcal{T}} := \sum_{k=1}^{ne} \int_{\partial\Omega_k} (\boldsymbol{a}^- - \boldsymbol{a}^+)\, b \, \mathrm{d}s.$$

With this, we can define the IMEX Runge-Kutta discontinuous Galerkin method we use in the following. Please note that we only give the definition of this method and refer to [17, 34] for more details. Furthermore, we only treat globally stiffly accurate IMEX Runge-Kutta methods here, these are methods where the last stage is identical to the update step [5].

Definition 1 (IMEX discontinuous Galerkin method)**.** *Let a globally stiffly accurate IMEX Runge-Kutta method be given by its Butcher tableau, terms with an overhat referring to the explicit part. Initial values for the equation are termed $\boldsymbol{w}^0$. For every $n = 0, \dots, N-1$ do the following:*

1. *For $i = 1, \dots, s$: Seek $\boldsymbol{w}^{n,i} \in V_q^{\dim+1}$ such that*

$$\begin{aligned} 0 = &\left(\boldsymbol{w}^{n,i} - \boldsymbol{w}^n, \varphi\right)_{\mathcal{T}} \\ &+ \Delta t^n \sum_{j=1}^{i} \widetilde{A}_{i,j} \left(-\left(\widetilde{\boldsymbol{f}}(\boldsymbol{w}^{n,j}), \nabla\varphi\right)_{\mathcal{T}} + \frac{1}{2}\left\{\widetilde{\boldsymbol{f}}(\boldsymbol{w}^{n,j}), \varphi\right\}_{\partial\mathcal{T}} + \frac{1}{2}\,\mathrm{Diag}\left\{\frac{1}{\varepsilon^2}, 1, \dots, 1\right\} [\![\boldsymbol{w}^{n,j}, \varphi]\!]_{\partial\mathcal{T}} \right) \\ &+ \Delta t^n \sum_{j=1}^{i-1} \widehat{A}_{i,j} \left(-\left(\widehat{\boldsymbol{f}}(\boldsymbol{w}^{n,j}), \nabla\varphi\right)_{\mathcal{T}} + \frac{1}{2}\left\{\widehat{\boldsymbol{f}}(\boldsymbol{w}^{n,j}), \varphi\right\}_{\partial\mathcal{T}} + \varepsilon\, [\![\boldsymbol{w}^{n,j}, \varphi]\!]_{\partial\mathcal{T}} \right) \end{aligned} \tag{4}$$

   holds for all $\varphi \in V_q$. The internal time instances are given by

$$\widetilde{t}^{n,j} := t^n + \widetilde{c}_j \Delta t^n, \qquad \text{and} \qquad \widehat{t}^{n,j} := t^n + \widehat{c}_j \Delta t^n.$$

2. *Set $\boldsymbol{w}^{n+1} := \boldsymbol{w}^{n,s}$.*

The used IMEX Runge-Kutta methods are summarized in Appendix A.

2.2. Splitting techniques

It is the intention of this paper to both extend the recently introduced RS-IMEX splitting and to compare these extensions against well-known splittings from literature. To this end, we start by defining an abstract splitting which unifies all splittings used in this work. In the sequel, we assume that $0 < \varepsilon < 1$. Note that the upper limit is arbitrary and can be changed by a simple rescaling of the equations.

Definition 2 (Generalized splitting)**.** *Let the smooth functions $\mathcal{M}$, $\mathcal{H}$ and $\mathcal{K}$ be given and assume that each of them can be represented by an asymptotic expansion in form*

$$\begin{aligned}\mathcal{M} &= \mathcal{M}_{(0)} + \varepsilon\mathcal{M}_{(1)} + \varepsilon^2\mathcal{M}_{(2)} + \mathcal{O}(\varepsilon^3),\\ \mathcal{H}(\rho) &= \mathcal{H}_{(0)}(\rho_{(0)}) + \varepsilon\mathcal{H}_{(1)}(\rho_{(0)},\rho_{(1)}) + \varepsilon^2\mathcal{H}_{(2)}(\rho_{(0)},\rho_{(1)},\rho_{(2)}) + \mathcal{O}(\varepsilon^3),\\ \mathcal{K}(\rho,\boldsymbol{u}) &= \mathcal{K}_{(0)}(\rho_{(0)},\boldsymbol{u}_{(0)}) + \mathcal{O}(\varepsilon).\end{aligned}$$

Let furthermore be $0 \le \mathcal{M}(\varepsilon) < 1$ for $\varepsilon < 1$. The functions $\mathcal{H}_{(0)}$ and $\mathcal{H}_{(1)}$ are supposed to fulfill

$$\nabla\mathcal{H}_{(0)}(\rho_{(0)}) = \mathcal{H}'_{(0)}(\rho_{(0)})\nabla\rho_{(0)},$$

with $\mathcal{H}'_{(0)}(\rho_{(0)}) > 0$ if $\rho_{(0)}$ being strictly positive and

$$\nabla\mathcal{H}_{(1)}(\rho_{(0)},\rho_{(1)}) = \mathcal{H}^*_{(1)}(\rho_{(0)})\nabla\rho_{(1)},$$

if $\rho_{(0)} \equiv$ const with $\mathcal{H}^*_{(1)}(\rho_{(0)}) > 0$. Building upon this, a unifiying generalized splitting is defined by

$$\widetilde{\boldsymbol{f}} := \begin{pmatrix}(1-\mathcal{M})\rho\boldsymbol{u}\\ \mathcal{K}(\rho,\boldsymbol{u}) + \frac{\mathcal{H}(\rho)}{\varepsilon^2}Id\end{pmatrix} \qquad \text{and} \qquad \widehat{\boldsymbol{f}} := \begin{pmatrix}\mathcal{M}\rho\boldsymbol{u}\\ \rho\boldsymbol{u}\otimes\boldsymbol{u} - \mathcal{K}(\rho,\boldsymbol{u}) + \frac{p(\rho)-\mathcal{H}(\rho)}{\varepsilon^2}Id\end{pmatrix}. \tag{5}$$

Remark 1. *The following remark on the splittings can be made:*

- *Obviously, this splitting is always consistent in the sense that $\widetilde{\boldsymbol{f}} + \widehat{\boldsymbol{f}} = \boldsymbol{f}$.*
- *$\mathcal{M}$, $\mathcal{K}$ and $\mathcal{H}$ should be chosen in such a way that both explicit and implicit parts are hyperbolic. There will always be a value $\varepsilon_0 > 0$ such that for all $\varepsilon < \varepsilon_0$ the implicit flux $\widetilde{f}$ induces a strictly hyperbolic system. The examples mentioned in this work will induce hyperbolic systems for both $\widehat{\boldsymbol{f}}$ and $\widetilde{\boldsymbol{f}}$ for all values of $0 < \varepsilon < 1$.*

We can cast the splittings used in this work into the above-mentioned framework:

1. Splitting by Degond/Tang [8]: Take

   $$\mathcal{M} = 0, \qquad \mathcal{K} = 0 \qquad \text{and} \qquad \mathcal{H} = \left(1-\varepsilon^2\right)p(\rho)$$

   in the generalized splitting.
2. Splitting by Haack/Jin/Liu [12]: Take

   $$\mathcal{M} = \varepsilon^2, \qquad \mathcal{K} = 0 \qquad \text{and} \qquad \mathcal{H} = a(t)\rho$$

   in (5) to obtain this splitting, where $a(t) := \min_{\boldsymbol{x}} p'(\rho(\boldsymbol{x},t))$. In the algorithm, the coefficient $a(t)$ is evaluated explicitly, i.e., for the implicit flux we use $a(t)$ evaluated at the previous stage.
3. RS-IMEX splitting [18]: For a given, so-called reference solution $\boldsymbol{w}_{\text{ref}}$, the RS-IMEX splitting is defined by setting

   $$\mathcal{M} = 0, \qquad \mathcal{K} = -\rho\boldsymbol{u}_{\text{ref}}\otimes\boldsymbol{u}_{\text{ref}} + \rho\boldsymbol{u}\otimes\boldsymbol{u}_{\text{ref}} + \boldsymbol{u}_{\text{ref}}\otimes\rho\boldsymbol{u} \qquad \text{and} \qquad \mathcal{H} = p(\rho_{\text{ref}}) + p'(\rho_{\text{ref}})(\rho_{\text{ref}} - \rho).$$

   The idea behind this splitting is a linearization of the convective fluxes around the reference solution $\boldsymbol{w}_{\text{ref}}$ and taking the remainder as explicit flux contribution. For details, we refer to [29, 18]. In previous works, we have always used the reference solution to be the solution to the incompressible equations, Equation (3), computed with the same order of accuracy as done for the compressible equation. In this work, we also present other choices, namely the following ones:

- RS-IMEX-$q_C q_I$: This is the most obvious simplification, namely the computation of the compressible solution with polynomial order q_C, while the incompressible solution is computed with polynomial order $q_I \leq q_C$.
- RS-IMEX-min: The reference solution is defined by

$$\boldsymbol{w}_{\text{ref}} := \min_{\boldsymbol{x}} \boldsymbol{w}(\boldsymbol{x}, t).$$

  This leads, of course, to a tremendous simplification, because the reference solution no longer requires the solution of the incompressible Euler equations. The minimum is evaluated explicitly.
- RS-IMEX-mean: In the same spirit, the following variant only uses $\rho_{(0)}$ (which can be extracted from the initial conditions without extra algorithmic work) and the mean value of $\boldsymbol{u}$:

$$\rho_{\text{ref}} := \rho_{(0)} \qquad \text{and} \qquad \boldsymbol{u}_{\text{ref}} = \frac{1}{|\Omega|} \int_\Omega \boldsymbol{u} \mathrm{d}x.$$

  This is also a tremendous simplification in comparison to the original RS-IMEX. The mean is evaluated explicitly.

Those three variants all have in common that the reference solution can by definition be written in an asymptotic expansion, i.e.,

$$\rho_{\text{ref}} = (\rho_{\text{ref}})_{(0)} + \varepsilon^2 (\rho_{\text{ref}})_{(2)} + O(\varepsilon^3) \qquad \text{and} \qquad \boldsymbol{u}_{\text{ref}} = (\boldsymbol{u}_{\text{ref}})_{(0)} + O(\varepsilon).$$

With this, it is easy to see that $\mathcal{M}$ and $\mathcal{K}$ fulfill all the necessary conditions. For $\mathcal{H}$ we obtain

$$\begin{aligned}\mathcal{H} = &\underbrace{p((\rho_{\text{ref}})_{(0)}) + p'((\rho_{\text{ref}})_{(0)})(\rho_{(0)} - (\rho_{\text{ref}})_{(0)})}_{=\mathcal{H}_{(0)}} + \varepsilon \underbrace{\left(p'((\rho_{\text{ref}})_{(0)})(\rho_{(1)})\right)}_{=\mathcal{H}_{(1)}} \\ &+ \varepsilon^2 \underbrace{\left(p'((\rho_{\text{ref}})_{(0)})(\rho_{(2)}) + p'((\rho_{\text{ref}})_{(0)})((\rho_{\text{ref}})_{(2)}) + p''((\rho_{\text{ref}})_{(0)})(\rho_{\text{ref}})_{(2)}\rho_{(0)})\right)}_{=\mathcal{H}_{(2)}} + O(\varepsilon^3).\end{aligned}$$

The quantity $\rho_{(0)}$ occurs linearly in $\mathcal{H}_{(0)}$, and so does the quantity $\rho_{(1)}$ in $\mathcal{H}_{(1)}$. The coefficients are strictly positive if only the reference solution is strictly positive which is the case in this setting. Therefore, also the conditions imposed on $\mathcal{H}_{(0)}$ and $\mathcal{H}_{(1)}$ are fulfilled.

3. Asymptotic consistency

In this chapter, we show the asymptotic preserving property [15, 16] that gives an indication whether a numerical method is able to handle compressible flows at low Mach numbers. More precisely, it is shown that the $\varepsilon \to 0$ limit of the discretization is a consistent discretization of the incompressible Euler equations. In the sequel, we always work with an asymptotic expansion of the numerical solution, i.e.,

$$\boldsymbol{w}^{n,i} = \boldsymbol{w}^{n,i}_{(0)} + \varepsilon \boldsymbol{w}^{n,i}_{(1)} + \varepsilon^2 \boldsymbol{w}^{n,i}_{(2)} + O(\varepsilon^3).$$

Obviously, for the well-prepared initial conditions, this is true.

Definition 3 (Asymptotic consistency)**.** *A numerical method for the isentropic Euler equations with well prepared initial data, see Equation 2, is called asymptotically consistent if the computed density ρ^n is given by*

$$\rho^n = \rho_{(0)} + \varepsilon^2 \rho^n_{(2)} + O(\varepsilon^3) \qquad \textit{for} \qquad n = 1, \ldots, N,$$

where $\rho_{(0)}$ is a constant defined by the initial conditions. Furthermore, the formal limit $\varepsilon \to 0$ is a consistent discretization of the incompressible Euler equations.

We show the asymptotic consistency of the IMEX DG method coupled to the generalized splitting introduced in Definition 2. For the RS-IMEX splitting this property has previously been shown in [17].

Remark 2. *In the following, internal stages of the IMEX Runge-Kutte method are investigated. Due to Definition 1, we allow IMEX Runge-Kutta methods where* $\widetilde{A}_{1,1} = 0$*, which comes down to setting the first internal stage equal to* $\boldsymbol{w}^n$*. Obviously, this stage does not have to be considered explicitly. We can therefore safely assume that, without loss of generality,* $\widetilde{A}_{i,i} \neq 0$ *by considering stages* $i > 1$ *if necessary.*

Theorem 1. *The IMEX DG method defined in Section 2 coupled with the generalized splitting given in Definition 2 is asymptotically consistent.*

Proof. This theorem is a straightforward consequence of the following lemmas. More precisely, Lemmas 1, 2 and 3 show that the density is still well-prepared. From Lemmas 4 and 5 one can conclude that the limiting method is a consistent discretization of the limiting equation. □

The asymptotic expansion of $\widetilde{\boldsymbol{f}}$ and $\widehat{\boldsymbol{f}}$ are given by

$$\widetilde{\boldsymbol{f}} = \varepsilon^{-2}\widetilde{\boldsymbol{f}}_{(-2)} + \varepsilon^{-1}\widetilde{\boldsymbol{f}}_{(-1)} + \dots, \qquad \text{and} \qquad \widehat{\boldsymbol{f}} = \varepsilon^{-2}\widehat{\boldsymbol{f}}_{(-2)} + \varepsilon^{-1}\widehat{\boldsymbol{f}}_{(-1)} + \dots,$$

where the corresponding coefficients for the implicit part are given by

$$\widetilde{\boldsymbol{f}}_{(-2)} = \begin{pmatrix} 0 \\ \mathcal{H}_{(0)}Id \end{pmatrix}, \quad \widetilde{\boldsymbol{f}}_{(-1)} = \begin{pmatrix} 0 \\ \mathcal{H}_{(1)}Id \end{pmatrix} \quad \text{and} \quad \widetilde{\boldsymbol{f}}_{(0)} = \begin{pmatrix} (1-\mathcal{M}_{(0)})(\rho\boldsymbol{u})_{(0)} \\ \mathcal{K}_{(0)} + \mathcal{H}_{(2)}Id \end{pmatrix},$$

and consequently for the explicit part

$$\widehat{\boldsymbol{f}}_{(-2)} = \begin{pmatrix} 0 \\ (p_{(0)} - \mathcal{H}_{(0)})Id \end{pmatrix}, \quad \widehat{\boldsymbol{f}}_{(-1)} = \begin{pmatrix} 0 \\ (p_{(1)} - \mathcal{H}_{(1)})Id \end{pmatrix} \quad \text{and} \quad \widehat{\boldsymbol{f}}_{(0)} = \begin{pmatrix} \mathcal{M}_{(0)}(\rho\boldsymbol{u})_{(0)} \\ (\rho\boldsymbol{u})_{(0)} \otimes \boldsymbol{u}_{(0)} - \mathcal{K}_{(0)} + (p_{(2)} - \mathcal{H}_{(2)})Id \end{pmatrix}.$$

The numerical flux function of the implicit part scales the stabilization of the conservation of mass equation with ε^{-2}. Due to this special numerical stabilization we can apply Lemma 2 of [17] and obtain that $\rho_{(0)}^{n,i}$ and $\rho_{(1)}^{n,i}$ are continuous over the whole domain.

Lemma 1. *The quantities* $\rho_{(0)}^{n,i}$ *and* $\rho_{(1)}^{n,i}$ *are continuous over the whole spatial domain under the assumptions of Theorem 1.*

Proof. The numerical stabilization are the only $O(\varepsilon^{-2})$ and $O(\varepsilon^{-1})$, respectively, terms in the discretization of mass equation. We can therefore apply the proof from [17, Lemma 2]. □

Lemma 2. *The quantities* $\rho_{(0)}^{n,i}$ *and* $\rho_{(1)}^{n,i}$ *are constant in space under the assumptions of Theorem 1.*

Proof. We consider the $O(\varepsilon^{-2})$ terms of the discretization of the conservation of momentum equation. After integration by parts, these terms are given by

$$\begin{aligned} 0 = &\sum_{j=1}^{i} \widetilde{A}_{i,j} \left[\left(\nabla \cdot \left(\mathcal{H}_{(0)}(\rho_{(0)}^{n,j}) Id \right), \varphi \right)_{\mathcal{T}} + \frac{1}{2} \left[\!\left[\mathcal{H}_{(0)}(\rho_{(0)}^{n,j}) \boldsymbol{n}_k, \varphi \right]\!\right]_{\partial\mathcal{T}} \right] \\ &+ \sum_{j=1}^{i-1} \widehat{A}_{i,j} \left[\left(\nabla \cdot \left(p'(\rho_{(0)}^{n,j}) - \mathcal{H}_{(0)}(\rho_{(0)}^{n,j}) Id \right), \varphi \right)_{\mathcal{T}} + \frac{1}{2} \left[\!\left[\left(p'(\rho_{(0)}^{n,j}) - \mathcal{H}_{(0)}(\rho_{(0)}^{n,j}) Id \right) \cdot \boldsymbol{n}_k, \varphi \right]\!\right]_{\partial\mathcal{T}} \right]. \end{aligned} \tag{6}$$

We assumed that the initial conditions and the previous time instances are well-prepared. Therefore we know that $\rho_{(0)}^{n,j}$ is constant in space for $j < i$. The equation thus reduces to

$$0 = \left(\nabla \mathcal{H}_{(0)}(\rho_{(0)}^{n,i}), \varphi \right)_{\mathcal{T}} + \frac{1}{2} \left[\!\left[\mathcal{H}_{(0)}(\rho_{(0)}^{n,i}) \boldsymbol{n}_k, \varphi \right]\!\right]_{\partial\mathcal{T}}. \tag{7}$$

The limiting density $\rho_{(0)}^{n,i}$ is continuous over the whole domain, see Lemma 1, therefore the boundary integrals sum up to zero and we obtain

$$0 = \left(\nabla \mathcal{H}_{(0)}(\rho_{(0)}^{n,j}), \varphi \right)_{\mathcal{T}} = \left(\mathcal{H}'_{(0)}(\rho_{(0)}^{n,i}) \nabla \rho_{(0)}^{n,i}, \varphi \right)_{\mathcal{T}}. \tag{8}$$

We consider the d^{th} equation in (8) and choose $\varphi = \partial_{\boldsymbol{x}_d}\rho^{n,i}_{(0)}$. Then, one obtains

$$0 = \left(\mathcal{H}'_{(0)}(\rho^{n,i}_{(0)})\partial_{\boldsymbol{x}_d}\rho^{n,i}_{(0)}, \partial_{\boldsymbol{x}_d}\rho^{n,i}_{(0)}\right)_{\mathcal{T}}.$$

Since we integrate over the whole domain and $\mathcal{H}'_{(0)}(\rho^{n,i}_{(0)})$ is strictly positive, we can conclude that

$$\partial_{\boldsymbol{x}_d}\rho^{n,i}_{(0)} = 0.$$

Thus $\rho_{(0)}$ is constant in space. In a completely similar way we obtain that $\rho^{n,i}_{(1)}$ is constant in space as well. □

Lemma 3. *The quantities $\rho^{n,i}_{(0)}$ and $\rho^{n,i}_{(1)}$ are constant in time under the assumptions of Theorem 1.*

Proof. We consider the $O(1)$ terms of the discretization of the conservation of mass equation,

$$\begin{aligned} 0 = &\left(\rho^{n,i}_{(0)} - \rho^{n}_{(0)}, \varphi\right)_{\mathcal{T}} + \Delta t^n \sum_{j=1}^{i} \widetilde{A}_{i,j}\left[-\left((1-\mathcal{M}_{(0)})\rho^{n,j}_{(0)}\boldsymbol{u}^{n,j}_{(0)}, \nabla\varphi\right)_{\mathcal{T}} + \frac{1}{2}\left(\left\{(1-\mathcal{M}_{(0)})\rho^{n,j}_{(0)}\boldsymbol{u}^{n,j}_{(0)}, \varphi\right\}_{\partial\mathcal{T}} + \left[\!\left[\rho^{n,j}_{(2)}, \varphi\right]\!\right]_{\partial\mathcal{T}}\right)\right] \\ &+ \Delta t^n \sum_{j=1}^{i-1} \widehat{A}_{i,j}\left[-\left(\mathcal{M}_{(0)}\rho^{n,j}_{(0)}\boldsymbol{u}^{n,j}_{(0)}, \nabla\varphi\right)_{\mathcal{T}} + \frac{1}{2}\left\{\mathcal{M}_{(0)}\rho^{n,j,-}_{(0)}\boldsymbol{u}^{n,j,-}_{(0)}, \varphi\right\}_{\partial\mathcal{T}}\right]. \end{aligned} \tag{9}$$

Due to Lemma 2 and by choosing $\varphi \equiv 1$ we obtain

$$0 = \left(\rho^{n,i}_{(0)} - \rho^{n}_{(0)}\right)(1,1)_{\mathcal{T}} + \frac{\Delta t^n}{2}\sum_{j=1}^{i}\widetilde{A}_{i,j}\left(\left\{(1-\mathcal{M}_{(0)})\rho^{n,j}_{(0)}\boldsymbol{u}^{n,j}_{(0)}, 1\right\}_{\partial\mathcal{T}} + \left[\!\left[\rho^{n,j}_{(2)}, 1\right]\!\right]_{\partial\mathcal{T}}\right) + \frac{\Delta t^n}{2}\sum_{j=1}^{i-1}\widehat{A}_{i,j}\left\{\mathcal{M}_{(0)}\rho^{n,j}_{(0)}\boldsymbol{u}^{n,j}_{(0)}, 1\right\}_{\partial\mathcal{T}}.$$

A periodic domain is assumed in this work, thus all boundary integrals sum up to zero. Overall we obtain

$$0 = \left(\rho^{n,i}_{(0)} - \rho^{n}_{(0)}\right)(1,1)_{\mathcal{T}} \qquad \Rightarrow \qquad \rho^{n,i}_{(0)} = \rho^{n}_{(0)}.$$

Thus, $\rho^{n,i}_{(0)}$ is constant in space and time. In a completely similar way we can show that also $\rho^{n,i}_{(1)}$ is constant in space and time. □

Remark 3. *For the ease of presentation, a periodic domain has been assumed. Yet, the above lemma can still be shown for a non-periodic domain given that one chooses suitable boundary conditions. E.g., for the proof of the above lemma, it would also suffice to use slip boundary conditions, i.e.,*

$$\int_{\partial\Omega} \boldsymbol{u}\cdot\boldsymbol{n}\mathrm{d}s = 0.$$

Lemma 4. *The $O(1)$ terms of the discretization of the conservation of mass equation are, under the assumptions of Theorem 1, a consistent discretization of*

$$\nabla\cdot\boldsymbol{u}_{(0)} = 0.$$

Proof. We consider again Equation (9) together with the results of Lemma 2 and 3:

$$\begin{aligned} 0 = &-\Delta t^n \sum_{j=1}^{i}\widetilde{A}_{i,j}\left((1-\mathcal{M}_{(0)})\boldsymbol{u}^{n,j}_{(0)}, \nabla\varphi\right)_{\mathcal{T}} - \Delta t^n\sum_{j=1}^{i-1}\widehat{A}_{i,j}\left(\mathcal{M}_{(0)}\boldsymbol{u}^{n,j}_{(0)}, \nabla\varphi\right)_{\mathcal{T}} \\ &+ \frac{\Delta t^n}{2}\sum_{j=1}^{i}\widetilde{A}_{i,j}\left(\left\{(1-\mathcal{M}_{(0)})\boldsymbol{u}^{n,j}_{(0)}, \varphi\right\}_{\partial\mathcal{T}} + \frac{1}{\rho_{(0)}}\left[\!\left[\rho^{n}_{(2)}, \varphi\right]\!\right]_{\partial\mathcal{T}}\right) + \frac{\Delta t^n}{2}\sum_{j=1}^{i-1}\widehat{A}_{i,j}\left\{\mathcal{M}_{(0)}\boldsymbol{u}^{n,j}_{(0)}, \varphi\right\}_{\partial\mathcal{T}}. \end{aligned} \tag{10}$$

This is directly a consistent implicit discontinuous Galerkin discretization of $\nabla\cdot\boldsymbol{u}_{(0)} = 0$. □

Lemma 5. *The $O(1)$ terms of the discretization of the conservation of momentum equation are, under the assumptions of Theorem 1, a consistent discretization of*

$$(\boldsymbol{u}_{(0)})_t + \nabla \cdot (\boldsymbol{u}_{(0)} \otimes \boldsymbol{u}_{(0)}) + \frac{\nabla p_{(2)}}{\rho_{(0)}} = 0.$$

Proof. We consider the $O(1)$ terms of the discretization of the momentum equation and directly divide by $\rho_{(0)}$,

$$\begin{aligned} 0 = &\left(\boldsymbol{u}_{(0)}^{n,i} - \boldsymbol{u}_{(0)}^{n}, \varphi\right)_{\mathcal{T}} + \Delta t^n \sum_{j=1}^{i} \widetilde{A}_{i,j} \left[-\left(\frac{\mathcal{K}_{(0)}^{n,j}}{\rho_{(0)}} + \frac{\mathcal{H}_{(2)}^{n,j} Id}{\rho_{(0)}}, \nabla\varphi \right)_{\mathcal{T}} + \frac{1}{2} \left\{ \frac{\mathcal{K}_{(0)}^{n,j}}{\rho_{(0)}} + \frac{\mathcal{H}_{(2)}^{n,j}}{\rho_{(0)}} Id, \varphi \right\}_{\partial\mathcal{T}} + \frac{1}{2} \left[\!\left[\boldsymbol{u}_{(0)}^{n,j}, \varphi \right]\!\right]_{\partial\mathcal{T}} \right] \\ &+ \Delta t^n \sum_{j=1}^{i-1} \widehat{A}_{i,j} \left[-\left(\boldsymbol{u}_{(0)}^{n,j} \otimes \boldsymbol{u}_{(0)}^{n,j} - \frac{\mathcal{K}_{(0)}^{n,j}}{\rho_{(0)}} + \frac{p_{(2)}^{n,j} - \mathcal{H}_{(2)}^{n,j}}{\rho_{(0)}} Id, \nabla\varphi \right)_{\mathcal{T}} + \frac{1}{2} \left\{ \boldsymbol{u}_{(0)}^{n,j} \otimes \boldsymbol{u}_{(0)}^{n,j} - \frac{\mathcal{K}_{(0)}^{n,j}}{\rho_{(0)}} + \frac{p_{(2)}^{n,j} - \mathcal{H}_{(2)}^{n,j}}{\rho_{(0)}} Id, \varphi \right\}_{\partial\mathcal{T}} \right] \end{aligned}$$

This is a consistent IMEX DG discretization of the limiting momentum equation, where

$$\frac{\mathcal{K}_{(0)}(\rho_{(0)}, \boldsymbol{u}_{(0)})}{\rho_{(0)}} + \frac{\mathcal{H}_{(2)}^{n,j}(\rho_{(0)}, \rho_{(1)}, \rho_{(2)}) Id}{\rho_{(0)}}$$

corresponds to the implicit part and

$$\boldsymbol{u}_{(0)}^{n,j} \otimes \boldsymbol{u}_{(0)}^{n,j} - \frac{\mathcal{K}_{(0)}^{n,j}(\rho_{(0)}, \boldsymbol{u}_{(0)})}{\rho_{(0)}} + \frac{\left(p_{(2)}^{n,j}(\rho_{(0)}, \rho_{(1)}, \rho_{(2)}) - \mathcal{H}_{(2)}^{n,j}(\rho_{(0)}, \rho_{(1)}, \rho_{(2)})\right) Id}{\rho_{(0)}}$$

corresponds to the explicit part. □

4. Numerical results

In this section, we evaluate the accuracy and efficiency of the different splitting techniques discussed in Section 2, cast into the generalized form given by Definition 2. Therefore, we consider two testcases: For the first example an exact solution is known and it can hence be used for the evaluation of accuracy and efficiency. The second testcase is more complex and no exact solution is known. Hence, it is employed only to indicate if a splitting is able to predict a complex three-dimensional behavior and to evaluate its efficiency.

Based on these testcases, in this section we aim to answer the following specific questions:

a) Do the splitting schemes differ in terms of accuracy? Given the unified form of the splitting techniques derived in this work and the common discretization by an IMEX discontinuous Galerkin discretization, what can be deduced about their computational efficiency?
b) For the novel RS-IMEX splitting schemes, what is the influence of choosing the reference solution as outlined in Section 2 on its properties?

Remark 4 (Solving the (non-)linear system of equations)**.** *As described in Section 2, a (depending on the splitting potentially non-linear) system of equations has to be solved for every IMEX Runge-Kutta stage. For this, we use a matrix-free Newton-GMRES method where the occurring Jacobian-vector product is approximated with a finite difference according to [28] and [23]. To gain computational efficiency a block-Jacobian preconditioner is equipped. A more detailed description of the solution strategy can be found in Section 4 of [34].*

Remark 5 (Computation of the reference solution)**.** *The reference solution for RS-IMEX-$q_C q_I$ requires the solution of the incompressible system with a polynomial ansatz of degree q_I which typically is different (smaller than) the degree q_C for the compressible solution. This introduces an algorithmic challenge in that two distinct discretization operators must exist in parallel during the computation (on the same grid) which are coupled uni-directionally via the reference solution.*

An elegant way of achieving this is running two instances of the framework, which communicate by message passing interfaces (MPI). Since the basis for the incompressible solution is of lesser degree than the compressible

one, the incompressible solution is communicated to minimize message size. Within the compressible solver, it is then interpolated onto the local grid via a precomputed Vandermonde matrix.

Note that in the following, we limit the investigations to the coarsest case of $q_I = 1$. Calculating the reference solution the artificial compressibility-type incompressible solver described in [34] is used. It is equipped with a fully implicit time discretization using the implicit part of the IMEX Runge-Kutta schemes. In the following we denote the RS-IMEX-$q_C q_I$ scheme with $q_C = q_I$ as RS-IMEX-standard. All other splittings except for the RS-IMEX-$q_C q_I$ are parallelized by distributing the elements evenly on the available processors.

Remark 6 (Implementation of HJL and DeTa splitting)**.** *As mentioned in Section 2, we use the proposed splittings by Haack/Jin/Liu [12] and Degond/Tang [8], cast them into the generalized form and discretize them by our high order IMEX Runge-Kutta DG framework. Originally, the authors of these splitting developed different discretization options relying strongly on the derivation of an elliptic equation for the density. Hence, we do not evaluate the efficiencies and accuracies of their schemes, but evaluate the idea of splitting the equations as proposed by the authors.*

4.1. Testcase 1: HOT-Vortex

The high order traveling vortex (HOT-vortex) can be seen as an extension of the vortex given by Bispen et al. [3] and it has been previously used in [17, 34] to investigate the transport properties of the schemes.

Definition 4 (2d HOT-vortex)**.** *The equation of state for pressure is defined by $p(\rho) = \frac{1}{2}\rho^2$. Initial conditions are periodic and given on domain $\Omega = [0,1]^2$:*

$$\rho(\boldsymbol{x}, t=0) = 2 + 250,000\varepsilon^2 \begin{cases} \frac{1}{2} e^{\frac{2}{\Delta r}} \Delta r - \mathrm{Ei}\left(\frac{2}{\Delta r}\right) & r < \frac{1}{2} \\ 0 & \textit{otherwise} \end{cases}$$

$$\boldsymbol{u}(\boldsymbol{x}, t=0) = \begin{pmatrix} 1/2 \\ 0 \end{pmatrix} + 500 \begin{pmatrix} \frac{1}{2} - \boldsymbol{x}_2 \\ \boldsymbol{x}_1 - \frac{1}{2} \end{pmatrix} \cdot \begin{cases} e^{\frac{1}{\Delta r}} & r < \frac{1}{2} \\ 0 & \textit{otherwise} \end{cases},$$

with $r := \sqrt{(\boldsymbol{x}_1 - \frac{1}{2})^2 + (\boldsymbol{x}_2 - \frac{1}{2})^2}$ *and* $\Delta r := r^2 - \frac{1}{4}$.

Ei denotes the exponential integral function

$$\mathrm{Ei}(x) := \int_{-\infty}^{x} \frac{e^t}{t} \mathrm{d}t.$$

We obtain the initialization of the incompressible solver, required for the RS-IMEX-standard and the RS-IMEX-$q_C q_I$, by setting $\varepsilon = 0$ in Definition 4 and $p_{(2)} = \kappa\gamma\rho_{(0)}^{\gamma-1}\rho_{(2)}$. The HOT-vortex example describes the constant advection of a vortex in $\boldsymbol{x}_1$-direction with a transport speed of 0.5, therefore the exact solution is given by a translation of the initial state as

$$\rho(\boldsymbol{x}, t) = \rho\left(\boldsymbol{x} - (0.5t, 0)^T, t = 0\right), \quad \boldsymbol{u}(\boldsymbol{x}, t) = \boldsymbol{u}\left(\boldsymbol{x} - (0.5t, 0)^T, t = 0\right). \tag{11}$$

To evaluate the accuracy of the numerical solution, we use the L^2-norm at end time T as error measurement

$$e_{\Delta x} := \|\boldsymbol{w}^N - \boldsymbol{w}(T)\|_{L^2(\Omega)},$$

where $\boldsymbol{w}^N$ denotes the numerical approximation at $T = t^N$ and $\boldsymbol{w}(T)$ denotes the corresponding exact solution given by Equation (11). The mesh parameter Δx is defined to be $\Delta x = 1/\sqrt[\dim]{ne}$.

Evaluation of accuracy. We consider this testcase for the Mach numbers $\varepsilon = 10^{-1}, 10^{-2}, 10^{-3}, 10^{-4}$ and compare the errors $e_{\Delta x}$ for the different splittings. For all calculations, the parameters of the linear solver and the time step were held constant. Here, we use a fourth order discretization in space and time ($q_C = 3$ with IMEX-ARK-4A2 from [25]). Note that the RS-IMEX-standard splitting scheme is the same as used in [34].

Figure 1 shows that there are only very slight differences between the different splittings concerning their errors and convergence properties. All considered schemes have the desired order of convergence. An exception is the DeTa splitting for $\varepsilon = 10^{-4}$ where no stable solution could be found as machine accuracy issues become dominant for the matrix-free implementation of the nonlinear scheme. Concluding, all the considered schemes show comparable errors and asymptotic consistency. For the evaluation of the efficiency, we can thus determine the required computational time on a single fixed mesh as done in the next paragraph.

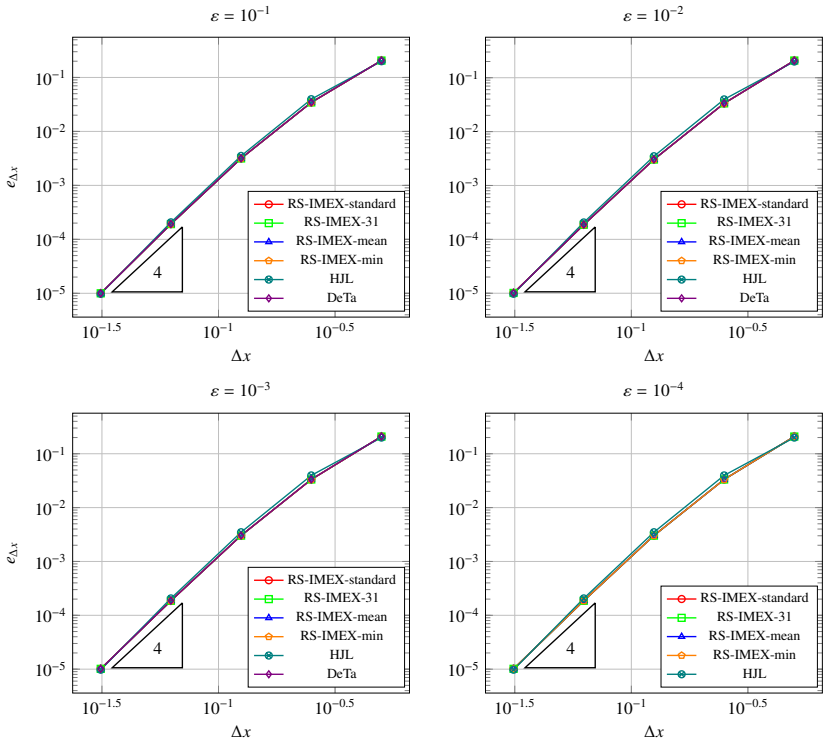

Figure 1: Overall convergence at different Mach numbers for HOT-Vortex with 4^{th} order ($q_C = 3$) discretization in space and time. Colors/symbols stand for different splitting methods; the triangles indicate the expected order of convergence. For $\varepsilon = 10^{-4}$, no stable solution could be found for the DeTa scheme as machine accuracy issues become dominant for the matrix-free implementation.

Evaluation of efficiency. For all calculations, the finest grid of Figure 1 with 32^2 elements is used and the computational costs are evaluated for a third and a fourth order spatial and temporal discretization ($q_C = 2$ with IMEX-ARS-443 by [1] and $q_C = 3$ with IMEX-ARK-4A2 by [25], respectively). The abort criteria of the linear and non-linear solvers are chosen to obtain the same residual reduction for the different schemes in each graph.

Figure 2 shows a qualitatively similar behavior for $q_C = 2$ and $q_C = 3$ with only slight differences: All linear schemes have a qualitatively similar behavior, showing convergence to a limit in computational time for a decreasing Mach number. It is visible that the HJL-splitting is in general as least as efficient as the fastest variant of the RS-IMEX splitting. In case that the matrix-free implementation is able to find a solution to the DeTa splitting, it will for 'large' ε be more efficient than the other approaches. As there are issues due to the matrix-free implementation, results for the DeTa scheme have not been plotted in Figure 2 for $q_C = 3$.

Evaluation of RS-IMEX reference solution variant. Regarding the differences between the RS-IMEX variants, we note from Figure 1 that no perceivable differences for the selected reference solution versions occur. In terms of computational resources (Figure 2), the RS-IMEX-mean and RS-IMEX-min are very similar but cheaper than the RS-IMEX-$q_C q_I$ variants. Moreover, RS-IMEX-$q_C q_I$ improves the RS-IMEX-standard scheme and for the $q_C = 2$ case is as efficient as RS-IMEX-mean for $\varepsilon = 10^{-4}$. Note that slight deviations of RS-IMEX-31 from the expected shape ($q_C = 3$ at $\varepsilon \leq 10^{-3}$) can be caused by the non optimized load balancing introduced by coupling the compressible and incompressible solver.

4.2. Testcase 2: Taylor-Green-Vortex

The Taylor-Green vortex was originally introduced in [31] and has been adopted to the non-dimensional isentropic Euler equations in [34]. The incompressible initialization field required for the standard RS-IMEX and the RS-IMEX-$q_C q_I$ scheme is given by

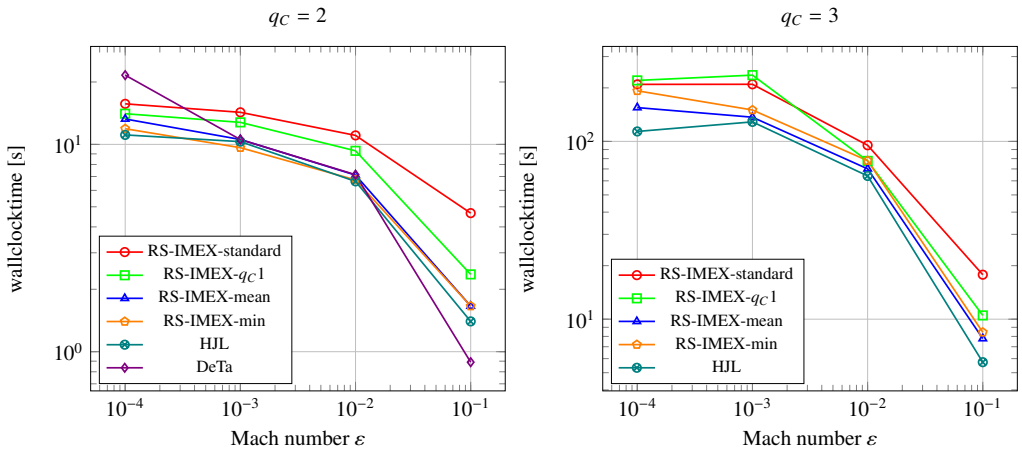

Figure 2: Comparison of computational time on 24 cores of different splittings for HOTVortex at different Mach numbers (left: 3^{rd} order, right: 4^{th} order). Again, for $q_C = 3$, the DeTa splitting is not plotted due to issues of the matrix-free implementation.

Definition 5 (Taylor-Green-Vortex (incompressible))**.** *Initial conditions of domain* $\Omega = [0, 2\pi]^3$ *with periodic boundary conditions:*

$$\rho_{(0)} = 1$$
$$\boldsymbol{u}_{(0)}(\boldsymbol{x}, t = 0) = V_0 \begin{pmatrix} \cos(\boldsymbol{x}_1)\cos(\boldsymbol{x}_2)\cos(\boldsymbol{x}_3) \\ -\cos(\boldsymbol{x}_1)\sin(\boldsymbol{x}_2)\cos(\boldsymbol{x}_3) \\ 0 \end{pmatrix}$$
$$p_{(2)}(\boldsymbol{x}, t = 0) = \frac{\rho_{(0)} V_0^2}{16}(\cos(2\boldsymbol{x}_1) + \cos(2\boldsymbol{x}_2))(\cos(2\boldsymbol{x}_3) + 2),$$

where V_0 *denotes a constant initial velocity which is chosen to be* $V_0 = 1$.

The compressible initialization is given by

Definition 6 (Taylor-Green-Vortex (compressible, isentropic))**.** *Initial conditions of domain* $\Omega = [0, 2\pi]^3$ *with periodic boundary conditions:*

$$\rho(\boldsymbol{x}, t = 0) = \rho_{(0)} + \varepsilon^2 \frac{V_0^2 {\rho_{(0)}}^{2-\gamma}}{16\gamma\kappa} (\cos(2\boldsymbol{x}_1) + \cos(2\boldsymbol{x}_2))(\cos(2\boldsymbol{x}_3) + 2),$$
$$\boldsymbol{u}(\boldsymbol{x}, t = 0) = V_0 \begin{pmatrix} \cos(\boldsymbol{x}_1)\cos(\boldsymbol{x}_2)\cos(\boldsymbol{x}_3) \\ -\cos(\boldsymbol{x}_1)\sin(\boldsymbol{x}_2)\cos(\boldsymbol{x}_3) \\ 0 \end{pmatrix}$$
$$p(\rho) = \frac{1}{2}\rho^2.$$

This inviscid testcase is used as an indicator if the splittings are able to predict a complex three-dimensional behavior. Secondly, we use it to evaluate the computational costs.

Evaluation of solution quality. We use a cartesian box with 16^3 elements, a polynomial degree of $q_C = 3$ and the IMEX-ARS-443 scheme from [1]. We consider the change of the scaled compressible kinetic energy

$$-\frac{1}{\varepsilon^2}\frac{\partial E_{kin,comp}}{\partial t} = -\frac{1}{2}\frac{\partial}{\partial t}\int_\Omega \rho \|\boldsymbol{u}\|_2^2 d\Omega,$$

as a measure for the dissipative properties of the schemes. For a perfectly resolved simulation, i.e., no discretization influence, it should remain zero. For the chosen resolution it can be expected that the kinetic energy remains constant and starts decreasing after some time.

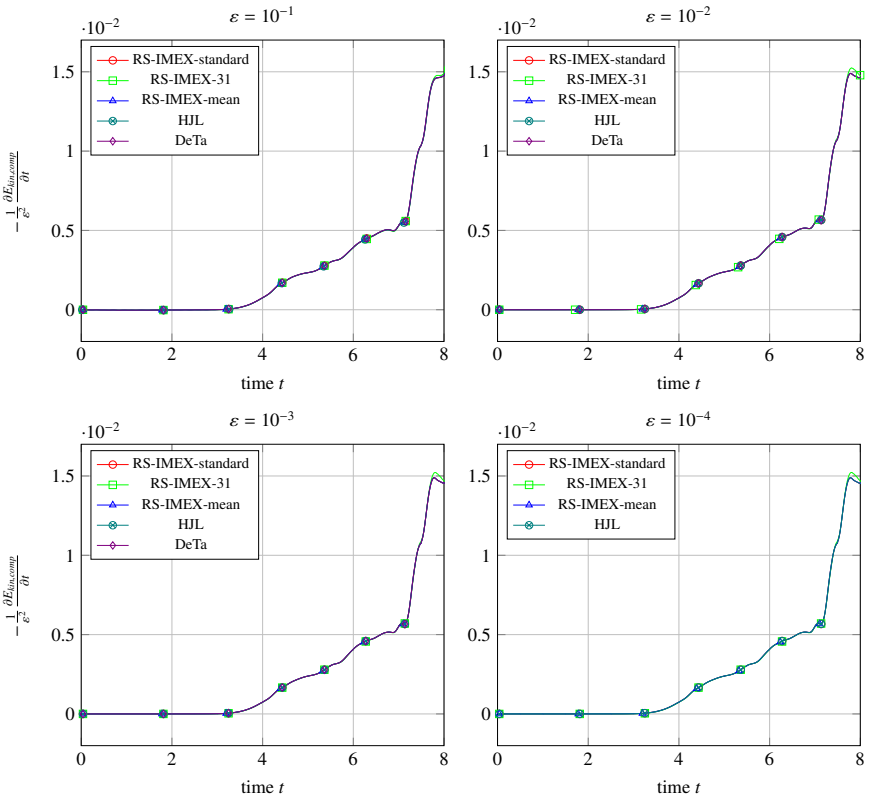

Figure 3: Scaled change rate of compressible kinetic energy for TGV with different splitting schemes (16^3 spatial elements, $q_C = 3$, IMEX-ARS-443) for different Mach numbers. Symbols additionally visualize superposing curves. Again, for $\varepsilon = 10^{-4}$, the DeTa splitting is not plotted due to issues of the matrix-free implementation.

Figure 3 illustrates that all considered splitting schemes have the same expected behavior. The results of the RS-IMEX-min are not displayed as large oscillations in the change rate of the kinetic energy are present. This instability can be cured by a smaller time step, indicating that for this more complex testcase, the choice of the reference solution could become more crucial than for the HOT-vortex. This issue warrants future study. In the following, we compare all splittings except for the RS-IMEX-min concerning their computational costs.

Evaluation of efficiency. As observed for the HOT-vortex in Figure 2, Figure 4 shows that the non-linear DeTa splitting is the most efficient scheme for $\varepsilon = 10^{-1}$, but here the least efficient for smaller Mach numbers. Again, all linear schemes converge to a limit in computational time for a decreasing Mach number. Here, the HJL-splitting is more efficient than the RS-IMEX schemes for $\varepsilon < 10^{-1}$. It is obvious that modifying the standard RS-IMEX scheme results in large savings in computational time but still remains computationally more costly than the HJL-splitting.

Evaluation of RS-IMEX reference solution variant. Comparing the RS-IMEX-standard with the RS-IMEX-31 scheme shows a nearly constant saving in computational costs, i.e., we see the savings calculating the incompressible solution on a lower polynomial degree, but do not see a Mach number dependent influence of a less accurate incompressible reference solution. The same results hold for the RS-IMEX-mean variant. Again, for $\varepsilon = 10^{-4}$ the RS-IMEX-mean and RS-IMEX-31 scheme are similar efficient.

Concluding remarks. The considered testcases show that in terms of accuracy, the particular choice of the splitting is not crucial, but can affect stability and efficiency. A splitting which is linear in the implicit part is beneficial for the considered matrix-free implementation and Mach numbers $\varepsilon \leq 10^{-2}$.

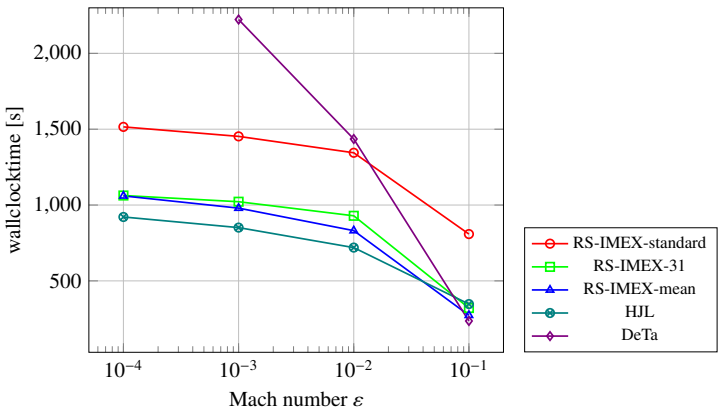

Figure 4: Comparison of computational time with 144 cores of different splittings for TGV at different Mach numbers (16^3 spatial elements, $q_C = 3$, IMEX-ARS-443). Again, for $\varepsilon = 10^{-4}$, the DeTa splitting is not plotted due to issues of the matrix-free implementation.

With the considered testcases it is not possible to identify the most efficient scheme as it differs for the two testcases.Nevertheless, the RS-IMEX-standard splitting scheme can be improved either using RS-IMEX-mean or RS-IMEX-$q_C q_I$. Especially if the calculation of the incompressible solution is computationally costly as for the Taylor-Green-Vortex, RS-IMEX-$q_C q_I$ can improve the standard RS-IMEX scheme. Choosing the minimum as a reference solution (RS-IMEX-min) for this testcase results in a less stable scheme, while the - comparably simple - RS-IMEX-mean variant was successful.

5. Conclusion and outlook

In the low Mach number limit, explicit time integration of the Euler equations becomes infeasible due to the prohibitively strict CFL condition. An established method of overcoming this limitation are flux splittings which aim at separating fast and slow waves without loss of hyperbolicity of the subsystems. In combination with IMEX time integrators, flux split formulations can then provide efficient and accurate discretizations in the low Mach number limit. A number of different formulations exist in literature, among them the RS-IMEX splitting presented in [17, 18, 29, 34], but the identification of the best approach is still elusive.

In this work, we have presented two contributions towards the goal of identifying and evaluating suitable splittings. Firstly, we have generalized the proof of asymptotic consistency for an IMEX discontinuous Galerkin method to a generalized splitting of the isentropic Euler equations. We have found that different splittings for the isentropic Euler equations, one given by Haack/Jin/Liu [12], one given by Degond/Tang [8] and three newly-developed ones based on the RS-IMEX splitting fit this generalized form and induce thus an asymptotically consistent overall numerical method.

Secondly, taking advantage of the generalized form of these splittings, we have established a numerical framework based on a discontinuous Galerkin discretization that allows side-by-side comparison of the splitting methods. Methods were compared with respect to accuracy and efficiency. We found that all splittings performed very similar in terms of accuracy for the considered two and three dimensional testcases. Regarding efficiency, the conclusions are not as clear-cut. The testcases showed that for $\varepsilon = 10^{-1}$ the splitting based on Degond/Tang [8] is most efficient. For smaller Mach numbers the splitting based on Haack/Jin/Liu [12] is most efficient but the RS-IMEX-mean scheme can compete in some cases.

Among the RS-IMEX schemes, the choice of the reference solution has a strong influence on computational time, with RS-IMEX-standard being the most expensive one and the RS-IMEX-mean leading to a considerable reduction in computational time without loss of accuracy. The RS-IMEX-min splitting has shown to be less stable than the other splittings.

Ongoing work deals with the extension of this work to other types of equations and the analytical investigation of uniform (in ε) convergence orders.

Acknowledgement

K. Kaiser has been partially supported by the German Research Foundation (DFG) through project NO 361/6-1; his study was supported by the Special Research Fund (BOF) of Hasselt University. J. Zeifang has been supported by the German Research Foundation (DFG) through the International Research Training Group GRK 2160/1: Droplet Interaction Technologies. We acknowledge the support and the computing time provided by the High Performance Computing Center Stuttgart (HLRS) through the *hpcdg* project.

Appendix A. IMEX Runge-Kutta methods

For the sake of completeness, we give the Butcher tableaux of the two IMEX Runge-Kutta methods used in this work, see Tables A.1-A.2.

0	0	0	0	0	0	0	0	0	0	0	0
1/2	0	1/2	0	0	0	1/2	1/2	0	0	0	0
2/3	0	1/6	1/2	0	0	2/3	11/18	1/18	0	0	0
1/2	0	-1/2	1/2	1/2	0	1/2	5/6	-5/6	1/2	0	0
1	0	3/2	-3/2	1/2	1/2	1	1/4	7/4	3/4	-7/4	0
	0	3/2	-3/2	1/2	1/2		1/4	7/4	3/4	-7/4	0

Table A.1: IMEX-ARS-443[1]. Left: implicit, right: explicit.

0	0	0	0	0	0	0	0	0	0	0	0	0	0	0	0
1/3	-1/6	1/2	0	0	0	0	0	1/3	1/3	0	0	0	0	0	0
1/3	1/6	-1/3	1/2	0	0	0	0	1/3	1/6	1/6	0	0	0	0	0
1/2	3/8	-3/8	0	1/2	0	0	0	1/2	1/8	0	3/8	0	0	0	0
1/2	1/8	0	3/8	-1/2	1/2	0	0	1/2	1/8	0	3/8	0	0	0	0
1	-1/2	0	3	-3	1	1/2	0	1	1/2	0	-3/2	0	2	0	0
1	1/6	0	0	0	2/3	-1/2	2/3	1	1/6	0	0	0	2/3	1/6	0
	1/6	0	0	0	2/3	-1/2	2/3		1/6	0	0	0	2/3	1/6	0

Table A.2: IMEX-ARK-4A2[25]. Left: implicit, right: explicit.

References

[1] U. M. Ascher, S. Ruuth, and R. Spiteri. Implicit-explicit Runge-Kutta methods for time-dependent partial differential equations. *Applied Numerical Mathematics*, 25:151–167, 1997.

[2] U. M. Ascher, S. Ruuth, and B. Wetton. Implicit-Explicit methods for time-dependent partial differential equations. *SIAM Journal on Numerical Analysis*, 32:797–823, 1995.

[3] G. Bispen, K. R. Arun, M. Lukáčová-Medvid'ová, and S. Noelle. IMEX large time step finite volume methods for low Froude number shallow water flows. *Communications in Computational Physics*, 16:307–347, 2014.

[4] S. Boscarino. Error analysis of IMEX Runge-Kutta methods derived from differential-algebraic systems. *SIAM Journal on Numerical Analysis*, 45:1600–1621, 2007.

[5] S. Boscarino, L. Pareschi, and G. Russo. Implicit-explicit Runge–Kutta schemes for hyperbolic systems and kinetic equations in the diffusion limit. *SIAM Journal on Scientific Computing*, 35(1):A22–A51, 2013.

[6] S. Boscarino, G. Russo, and L. Scandurra. All Mach number second order semi-implicit scheme for the Euler equations of gasdynamics. *arXiv preprint arXiv:1706.00272*, 2017.

[7] F. Cordier, P. Degond, and A. Kumbaro. An asymptotic-preserving all-speed scheme for the Euler and Navier-Stokes equations. *Journal of Computational Physics*, 231:5685–5704, 2012.

[8] P. Degond and M. Tang. All speed scheme for the low Mach number limit of the isentropic Euler equation. *Communications in Computational Physics*, 10:1–31, 2011.

[9] G. Dimarco, R. Loubère, and M.-H. Vignal. Study of a new asymptotic preserving scheme for the Euler system in the low Mach number limit. *SIAM Journal on Scientific Computing*, 39(5):A2099–A2128, 2017.

[10] M. Feistauer, V. Dolejší, and V. Kučera. On the discontinuous Galerkin method for the simulation of compressible flow with wide range of Mach numbers. *Computing and Visualization in Science*, 10(1):17–27, 2007.

[11] M. Feistauer and V. Kučera. On a robust discontinuous Galerkin technique for the solution of compressible flow. *Journal of Computational Physics*, 224(1):208–221, 2007.

[12] J. Haack, S. Jin, and J.-G. Liu. An all-speed asymptotic-preserving method for the isentropic Euler and Navier-Stokes equations. *Communications in Computational Physics*, 12:955–980, 2012.
[13] F. Hindenlang, G. Gassner, C. Altmann, A. Beck, M. Staudenmaier, and C.-D. Munz. Explicit discontinuous Galerkin methods for unsteady problems. *Computers and Fluids*, 61:86–93, 2012.
[14] D. Iampietro, F. Daude, P. Galon, and J.-M. Hérard. A weighted splitting approach for low-Mach number flows. In *International Conference on Finite Volumes for Complex Applications*, pages 3–11. Springer, 2017.
[15] S. Jin. Efficient asymptotic-preserving (AP) schemes for some multiscale kinetic equations. *SIAM Journal on Scientific Computing*, 21:441–454, 1999.
[16] S. Jin. Asymptotic preserving (AP) schemes for multiscale kinetic and hyperbolic equations: A review. *Rivista di Matematica della Universita Parma*, 3:177–216, 2012.
[17] K. Kaiser and J. Schütz. A high-order method for weakly compressible flows. *Communications in Computational Physics*, 22(4):1150–1174, 2017.
[18] K. Kaiser, J. Schütz, R. Schöbel, and S. Noelle. A new stable splitting for the isentropic Euler equations. *Journal of Scientific Computing*, 70:1390–1407, 2017.
[19] C. A. Kennedy and M. H. Carpenter. Additive Runge-Kutta schemes for convection-diffusion-reaction equations. *Applied Numerical Mathematics*, 44:139–181, 2003.
[20] S. Klainerman and A. Majda. Singular limits of quasilinear hyperbolic systems with large parameters and the incompressible limit of compressible fluids. *Communications on Pure and Applied Mathematics*, 34:481–524, 1981.
[21] R. Klein. Semi-implicit extension of a Godunov-type scheme based on low Mach number asymptotics I: One-dimensional flow. *Journal of Computational Physics*, 121:213–237, 1995.
[22] R. Klein, N. Botta, T. Schneider, C.D. Munz, S. Roller, A. Meister, L. Hoffmann, and T. Sonar. Asymptotic adaptive methods for multi-scale problems in fluid mechanics. *Journal of Engineering Mathematics*, 39(1):261–343, 2001.
[23] D. A. Knoll and D. E. Keyes. Jacobian-free Newton–Krylov methods: a survey of approaches and applications. *Journal of Computational Physics*, 193:357–397, 2004.
[24] D. A. Kopriva. *Implementing Spectral Methods for Partial Differential Equations: Algorithms for Scientists and Engineers*. Springer Publishing Company Incorporated, 1st edition, 2009.
[25] H. Liu and J. Zou. Some new additive Runge–Kutta methods and their applications. *Journal of Computational and Applied Mathematics*, 190(1-2):74–98, 2006.
[26] G. Métivier and S. Schochet. The incompressible limit of the non-isentropic Euler equations. *Archive for Rational Mechanics and Analysis*, 158(1):61–90, 2001.
[27] S. Noelle, G. Bispen, K. R. Arun, M. Lukáčová-Medvid'ová, and C.-D. Munz. A weakly asymptotic preserving low Mach number scheme for the Euler equations of gas dynamics. *SIAM Journal on Scientific Computing*, 36:B989–B1024, 2014.
[28] N. Qin, D. K. Ludlow, and S. T. Shaw. A matrix-free preconditioned Newton/GMRES method for unsteady Navier-Stokes solutions. *International Journal for Numerical Methods in Fluids*, 33:223–248, 2000.
[29] J. Schütz and K. Kaiser. A new stable splitting for singularly perturbed ODEs. *Applied Numerical Mathematics*, 107:18–33, 2016.
[30] J. Schütz and S. Noelle. Flux splitting for stiff equations: A notion on stability. *Journal of Scientific Computing*, 64(2):522–540, 2015.
[31] G. I. Taylor and A. E. Green. Mechanism of the production of small eddies from large ones. *Proceedings of the Royal Society of London. Series A, Mathematical and Physical Sciences*, 158(895):499–521, 1937.
[32] E. Turkel. Preconditioned methods for solving the incompressible and low speed compressible equations. *Journal of Computational Physics*, 72(2):277 – 298, 1987.
[33] W-A. Yong. A note on the zero Mach number limit of compressible Euler equations. *Proceedings of the American Mathematical Society*, 133(10):3079–3085, 2005.
[34] J. Zeifang, K. Kaiser, A. Beck, J. Schütz, and C.-D. Munz. Efficient high-order discontinuous Galerkin computations of low Mach number flows. *UHasselt CMAT Preprint UP-17-04*, 2017.